

# Use of the Geostrophic Approximation to Estimate Time-Varying Zonal Currents at the Equator

JOËL PICAUT

Groupe SURTROPAC, Institut Français de Recherche Scientifique pour le Développement en Coopération (ORSTOM), Nouméa, New Caledonia

STANLEY P. HAYES AND MICHAEL J. MCPHADEN

Pacific Marine Environmental Laboratory, National Oceanic and Atmospheric Administration, Seattle, Washington

Moored thermistor chains at 2°N and 2°S and current-temperature moorings at 0° are used to examine the accuracy of geostrophically estimated zonal velocity on the equator in the eastern (110°W) and western (165°E) Pacific. The meridionally differentiated form of the geostrophic balance is used to eliminate large errors due to wind-balanced cross-equatorial pressure gradients. Statistical analyses indicate that for time scales longer than 30–50 days, the observed and geostrophically estimated zonal velocities are similar (correlation coefficients of 0.6–0.9 and comparable amplitudes). Thus low-frequency equatorial current oscillations are reasonably well represented by the geostrophic approximation. However, the mean currents are poorly resolved with the available array. In the eastern Pacific the mean zonal speed difference over the 10-month comparison period is 25 cm s<sup>-1</sup> at 25 m and increases to 60 cm s<sup>-1</sup> at 125 m. At 165°E mean differences in the upper 250 m are typically 50 cm s<sup>-1</sup> over a 4-month record. The principal reason for these large mean differences is that the meridional scale of the mean currents is smaller than the spacing of the moorings. Comparison of observed and geostrophic velocity profiles obtained from shipboard sampling indicates that meridional spacing of about 1° latitude would be optimum for estimating the zonal velocity.

## 1. INTRODUCTION

Linear and nonlinear theories of the steady state equatorial circulation indicate that the geostrophic approximation should be applicable to zonal flow in the Equatorial Undercurrent (EUC) and South Equatorial Current (SEC) at the equator [McCreary, 1981; McPhaden, 1981; Pedlosky, 1987]. Also, linear equatorial wave theory predicts that zonal currents associated with long Rossby and Kelvin waves will be geostrophically balanced at the equator [Moore and Philander, 1977]. For observed Väisälä frequency profiles in the tropics, Rossby waves can exist at periods longer than about 1 month, and Kelvin waves can exist at all periods.

The geostrophic balance

$$\rho f u + p_y = 0 \quad (1)$$

is of no practical use right at the equator for estimating zonal currents, however, because it is indeterminate. Moreover, very close to the equator, observational noise and small deviations from geostrophy can give rise to cross-equatorial pressure gradients, which would lead to computational singularities using (1). Hence several authors have suggested use of the meridionally differentiated form of the geostrophic equation

$$\rho \beta u = -p_{yy} \quad (2)$$

to estimate zonal currents ( $u$ ) right at the equator [Jerlov, 1953; Tsuchiya, 1955a; Hidaka, 1955]. Colin and Rotschi [1970] obtained a reasonable estimate of the EUC using the mean of 10 hydrographic sections in the western Pacific using (2). Lukas and Firing [1984] demonstrated that the mean EUC estimated from 41 sections collected in the central Pacific during the 16-month NORPAX (North Pacific Experiment)

Hawaii-to-Tahiti Shuttle Experiment was nearly in geostrophic balance. However, Wyrki [1983], using a Gaussian function to estimate the curvature of the meridional pressure field, was unable to verify the geostrophic balance on each individual shuttle section. Johnson *et al.* [1988] continued the investigation of near-equatorial geostrophy during the NORPAX experiment by comparing geostrophic velocity estimates with underway velocity measurements from a Doppler acoustic log. In agreement with the earlier studies, they found that the mean flow was roughly in geostrophic balance but that the time dependent flow was not. This study stressed the importance of space-time smoothing in order to reduce the contribution of small-scale, high-frequency ageostrophic motions. Meridional smoothing has been studied by Hayes [1982] and Moum *et al.* [1987]. Hayes (1982) found that observed EUC speed in the eastern Pacific could be estimated to within 20% on four densely resolved (25-km spacing) meridional sections between 1°N and 1°S. Moum *et al.* [1987] investigated the required meridional resolution more thoroughly using continuous velocity profiling and density profiles every 1 km. They concluded that on their single section the EUC was in geostrophic balance and that optimal sampling of the EUC required 20-km station spacing and smoothing over 100 km.

All these studies point out the difficulty in obtaining accurate current estimates in view of the sensitivity of the equatorial geostrophic equation to small changes in the dynamic height. For example, a 1 dyn cm height difference between the equator and 1° due to high-frequency internal waves and tides [e.g., Hayes, 1982; Chereskin *et al.*, 1986] would lead to an erroneous estimate for zonal geostrophic current of 70 cm s<sup>-1</sup>. Either spatial or temporal smoothing is required in order to reduce the magnitude of these errors.

In the present paper, meridional arrays of thermistor chains and current meter moorings are used to investigate the limitations of the geostrophic relation for estimating the zonal equatorial currents. These continuous records permit the de-

Copyright 1989 by the American Geophysical Union.

Paper number 88JC03930.

0148-0227/89/88JC-03930\$05.00

ORSTOM Fonds Documentaire

N° : 30105, ex 1

Cote : B

TABLE 1. Vertical Array of Temperature Sensors for Moorings at 2°N, 0°, and 2°S at 110°W and 165°E

Latitude	Depth, m
<i>110°W (June 1, 1986, to April 10, 1987)</i>	
2°N/2°S	0, 20, 40, 60, 80, 100, 120, 140, 180, 300, 500
0°	0, 10,* 25,* 35, 45,* 60, 80,* 100, 120,* 160,* 200, 250*
<i>165°E (December 13, 1986, to April 18, 1987)</i>	
2°N/2°S	0, 50, 100, 125, 150, 175, 200, 225, 250, 300, 500
0°	0, 10, 30, 50,* 75, 100,* 125, 150, 175, 200,* 225, 250,* 300,* 400, 500

\*Velocity measurements were also taken at these depths.

termination of the temporal scales on which the geostrophic approximation is useful (given the spatial scales set by the mooring separations) and allow use of time averaging to reduce contamination by high-frequency noise. The temperature and velocity data are discussed in section 2. Application of the geostrophic balance is described in section 3, and the results are discussed in section 4.

2. DATA SOURCES AND PROCESSING

The moored and profiling observations used in this study were located in the eastern (110°W) and western (165°E) Pacific. Autonomous temperature line acquisition system (ATLAS) moored thermistor chains were located at 2°N and 2°S, and current-temperature moorings were at the equator along these longitudes. Sections of temperature and salinity obtained from shipboard conductivity-temperature-depth (CTD) profiles were collected as part of the Equatorial Pacific Ocean Climate Studies (EPOCS) and Surveillance Trans-Océanique du Pacifique (SURTROPAC) projects. They are used to establish the temperature-salinity (T-S) relations at the mooring sites and to investigate spatial structures in the vicinity of the moorings. The SURTROPAC measurements also included profiling current meter sections.

2.1. ATLAS Moorings

The ATLAS moored thermistor chain [Milburn and McLain, 1986] measures ocean temperature at 11 depths from 0 to 500 m (Table 1). Surface winds and air temperature are also recorded. Data are averaged over 2 hours (the mooring at 2°S, 165°E was averaged over only 1 hour) and telemetered to shore in near real time via the Argos satellite system.

Along 110°W the time series at all depths (Table 1) extended 313 days, from June 1, 1986, to April 10, 1987 (a 2-week gap in November 1986 was filled by linear interpolation). Along 165°E, 127 days of data from December 13, 1986, to April 18, 1987, were used (Table 1). Note that thermistor depths at the eastern and western locations differ in order to account for differences in the mean vertical thermal structure. In the analysis all ATLAS temperature time series were linearly interpolated in the vertical in order to obtain estimates at the depths of the equatorial current measurements. The basic time series used here are daily averages of these data.

2.2. Equatorial Current Meter Moorings

The current meter mooring data used in this study were collected at 110°W as part of the EPOCS program [Halpern, 1987a; McPhaden and Taft, 1988] and at 165°E as part of the U.S.-People's Republic of China bilateral air-sea interaction program [McPhaden et al., 1988]. Each surface mooring was instrumented in the upper 250-300 m with seven vector

averaging current meters (VACMs), which record 15-min average currents and temperatures. Seven (four) additional depths were instrumented at 165°E (110°W) with temperature recorders (Table 1).

Data were processed to daily averages in a manner similar to that described by Freitag et al. [1987]. A relatively short gap in 10-m currents at 110°W from September 19 to October 2, 1986, has been filled by extrapolation of 25-m currents using linear regression coefficients derived from overlapping time series. Zonal currents at these two levels have a correlation coefficient of 0.95 over a 138-day subset of the data. The 80-m current meter at 110°W failed between July 3 and November 5, 1986, and was filled with data at 80 m from a mooring at 108°W for the same time period. Coherence between variability at 108°W and 110°W at this depth is above the 95% significance level for periods greater than 7 days [Halpern, 1987a].

VACM instrumental errors for current measurements from a surface mooring in the Equatorial Undercurrent are expected to be less than 10 cm s<sup>-1</sup> [Halpern, 1987b].

2.3. Hydrographic and Current Profiler Data

Since 1979, several CTD sections have been collected along 110°W as part of the EPOCS program [Hayes et al., 1983]. Acquisition and processing of these data are discussed by Mangum et al. [1980]. On the recent cruises, vertical profiles of horizontal velocity are also collected using a hull-mounted acoustic Doppler current profiler [Feely et al., 1987]. These profiles generally extend to about 300 m. Figure 1 shows the mean temperature section along 110°W based on 10 cruises in 1979-1981 and 1984-1986. A representative zonal velocity sec-

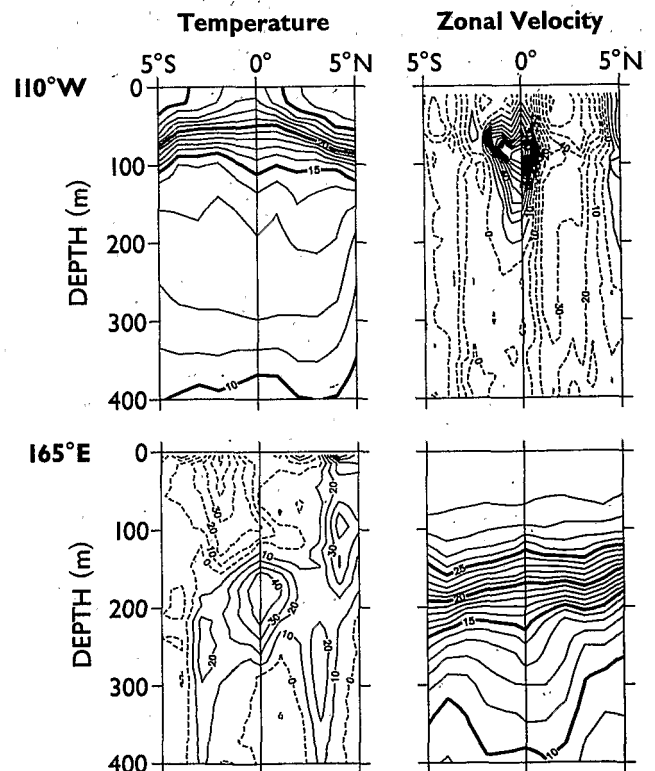


Fig. 1. Temperature and velocity sections at 110°W and at 165°E. At 110°W an average temperature section based on data from 10 cruises is shown; the velocity section is from a single transect in November 1986. At 165°E, temperature and velocity sections are the average of six cruises.

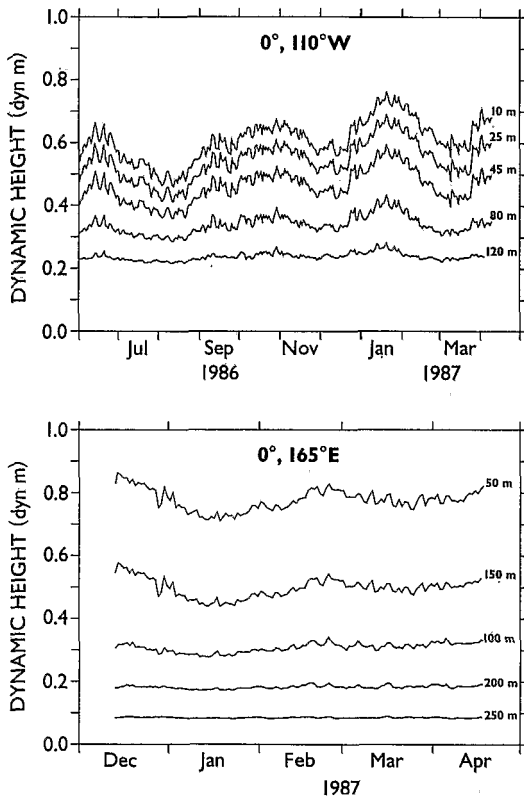


Fig. 2. Time series of daily estimates of equatorial dynamic height relative to 250 dbar at 110°W and relative to 300 dbar at 165°E. Estimates were computed from moored temperature measurements using  $T$ - $S$  relations as discussed in text.

tion (November 1986) is also shown. The temperature section is characterized by the upwelling and spreading of the thermocline at the equator and the relatively warm water north of the equator. The zonal velocity section shows an equatorial undercurrent centered slightly south of the equator with a maximum speed of about  $100 \text{ cm s}^{-1}$  at 90 m depth. Surface current was westward in the South Equatorial Current.

Since 1984, semiannual CTD and current profiler sections have been made from 20°S to 10°N along the 165°E meridian as part of the French Tropical Ocean and Global Atmosphere (TOGA)-SURTROPAC program. The current profiler is an Aanderaa-Tareq type which freely falls along a cable under a drifting buoy. The currents are calculated relative to the 600-m reference level. Details concerning the data acquisition and processing and some scientific results from the first six cruises (January 1984 to June 1986) are given by Delcroix *et al.* [1987]. Figure 1 shows the mean temperature and zonal current component for these six cruises. The thermocline is relatively deep and is marked by the presence of an EUC with a mean speed of  $50 \text{ cm s}^{-1}$  at 180-m depth. The mean SEC in the surface layer is not very well defined at the equator because of the presence of a strong eastward surface jet in January 1985 [Delcroix *et al.*, 1987]. From Figure 1 one can see that the EUC at 110°W and 165°E is mostly confined to within 2° latitude of the equator.

#### 2.4. Dynamic Height Calculation

Continuous time series of dynamic height are deduced from the moored temperature time series using mean  $T$ - $S$  curves based on the mean of 10 EPOCS and 6 SURTROPAC sec-

tions used in Figure 1. Only CTD stations at the mooring sites were used. Deviations from the mean  $T$ - $S$  relationship, particularly in the mixed layer, could introduce some errors in the near-surface dynamic height calculation. Kessler and Taft [1987] propose a scheme, using sea surface salinity, which improves such calculation above the thermocline in the central Pacific. Delcroix *et al.* [1987] discuss this problem in the western Pacific. No moored salinity time series were available to adjust the mean  $T$ - $S$  curve; thus  $T$ - $S$  fluctuations are a source of error in our dynamic height and therefore in geostrophic velocity. The magnitude of this error is estimated in section 4.

Temperatures from the thermistor chain and current meter moorings are calibrated to an accuracy of  $O(0.01^\circ\text{C})$ . The corresponding errors are random from one depth to the next, so errors in dynamic height based strictly on temperature sensor calibration will be only  $O(0.1 \text{ dyn cm})$ . Such an estimate is probably of an order of magnitude less than other errors in dynamic height introduced by the relatively poor vertical resolution of the temperature sensors and by use of the mean  $T$ - $S$  to estimate salinity.

Figure 2 shows daily time series of dynamic height on the equator at 110°W and 165°E, relative to 250 dbar and 300 dbar, respectively. At 110°W, oscillations with periods of 3–4 months and peak-to-trough amplitudes greater than 0.15 dyn m are apparent. Intraseasonal variations with similar periods though smaller amplitudes are evident at other times at 110°W [McPhaden and Taft, 1988]. Enhanced amplitudes in Figure 2 may be related to the occurrence of the 1986–1987 El Niño, which appears as a maximum dynamic height in January 1987. Higher-frequency energy is evident at 110°W as well, most notably at periods near 10 days. The 165°E dynamic height time series show similar high-frequency oscillations but with lower amplitude.

### 3. COMPARISON OF CALCULATED AND OBSERVED CURRENTS

#### 3.1. Use of the First Derivative of the Pressure Field

At both the 110°W and 165°E meridians, the continuous time series of dynamic height at 2°N, the equator, and 2°S were first used to calculate the geostrophic currents at 1°N and 1°S using the geostrophic equation (1). Representative near surface currents are shown in Figure 3. Along 110°W a strong shear between the 1°N and 1°S geostrophic currents is apparent. The 25-m mean velocity at 1°N was  $-100 \text{ cm s}^{-1}$  compared with  $50 \text{ cm s}^{-1}$  at 1°S. This geostrophic shear is the signature of the mean meridional pressure slope in the surface layers of the eastern equatorial Pacific [Lukas, 1981]. As Joyce [1988] has shown, however, this slope is balanced primarily by the meridional wind stress, so that geostrophic current estimates using (1) will be in error. Along 165°E, mean meridional wind and hence the mean meridional pressure slope are weak or absent, so there is no obvious shear between the 1°N and 1°S geostrophic currents.

#### 3.2. Use of the Second Derivative of the Pressure Field

We approximate the second derivative of the pressure field using the array measurements with second-order finite differences:

$$p_{yy} = [p(2^\circ\text{N}) + p(2^\circ\text{S}) - 2p(0^\circ)]/\Delta y^2$$

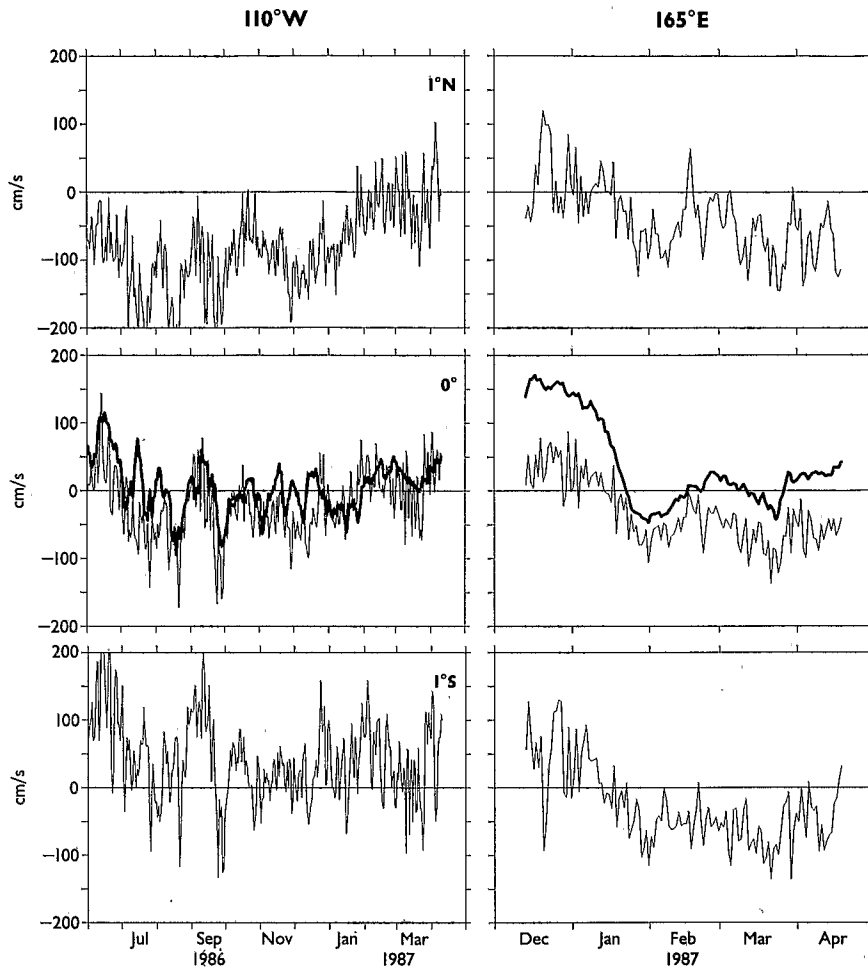


Fig. 3. Near surface geostrophic zonal currents at 1°N and 1°S estimated using (1). At the equator, geostrophic zonal current estimated using (2) (thin line) and observed zonal current (thick line) are shown. Currents are relative to 250 m at 110°W and 300 m at 165°E.

Note that with this particular finite difference scheme, the current at the equator is equivalent to the mean of geostrophic currents at 1°N and 1°S using (1). Estimates of zonal geostrophic flow at the equator using the finite difference version of (2) are shown in Figure 3. The reference levels for the dynamic height time series at 110°W (250 dbar) and at 165° (300 dbar) correspond to the deepest common level of temperature and current measurements; hence the calculated current is compared to the observed current relative to the same reference level. It is apparent from Figure 3 that low-frequency fluctuations calculated from (2) are qualitatively similar to observed currents at the equator.

Figure 4 shows examples of energy, coherence, and phase spectra for calculated and observed currents at selected depths at 110°W and 165°E. Energy spectra of observed and calculated currents are red at low frequency and indistinguishable from one another at the 95% level of confidence. Conversely, spectra of calculated currents show significantly elevated energy levels at periods shorter than about 10 days relative to the observed current spectra. This high-frequency energy is incoherent, in contrast to energy at periods longer than about 30–50 days which is typically in phase and significantly coherent at the 95% level of confidence.

Time series of calculated and observed currents at the equator were smoothed with a 21-day Hanning filter to remove

incoherent high frequencies (Figure 5). Low-frequency fluctuations have a similar time history at both locations, even at shallow levels where frictional influences are important (see section 4.4). Note that there are mean offsets, however, and at times the observed and calculated mean surface currents can be in opposite directions. Also, at the beginning of the 165°E record, the difference between observed and geostrophically estimated flow exceeds  $100 \text{ cm s}^{-1}$ .

Figure 6 summarizes the mean and standard deviation of the filtered observed and calculated current time series as a function of depth. Observed mean currents are more strongly eastward at all depths. The EUC speed core at both locations barely exceeds  $20 \text{ cm s}^{-1}$ , for example, compared with observed speeds of about  $80 \text{ cm s}^{-1}$ . Mean 50-m flow in the SEC at 165°E is directed opposite to the observed flow, and the difference between the two is close to  $70 \text{ cm s}^{-1}$ . At 110°W, the sign of the observed and calculated SEC agrees, but the calculated near-surface flow overestimates the observed flow by about  $25 \text{ cm s}^{-1}$ . Possible explanations of these discrepancies will be presented in the following section.

Observed and geostrophically estimated standard deviations at 110°W range between about 10 and  $30 \text{ cm s}^{-1}$ . Differences between the two are  $< 10 \text{ cm s}^{-1}$ , and the correlation between the time series is 0.6–0.9. At 165°E, estimated standard deviations are too weak by  $20 \text{ cm s}^{-1}$  at 50 m and

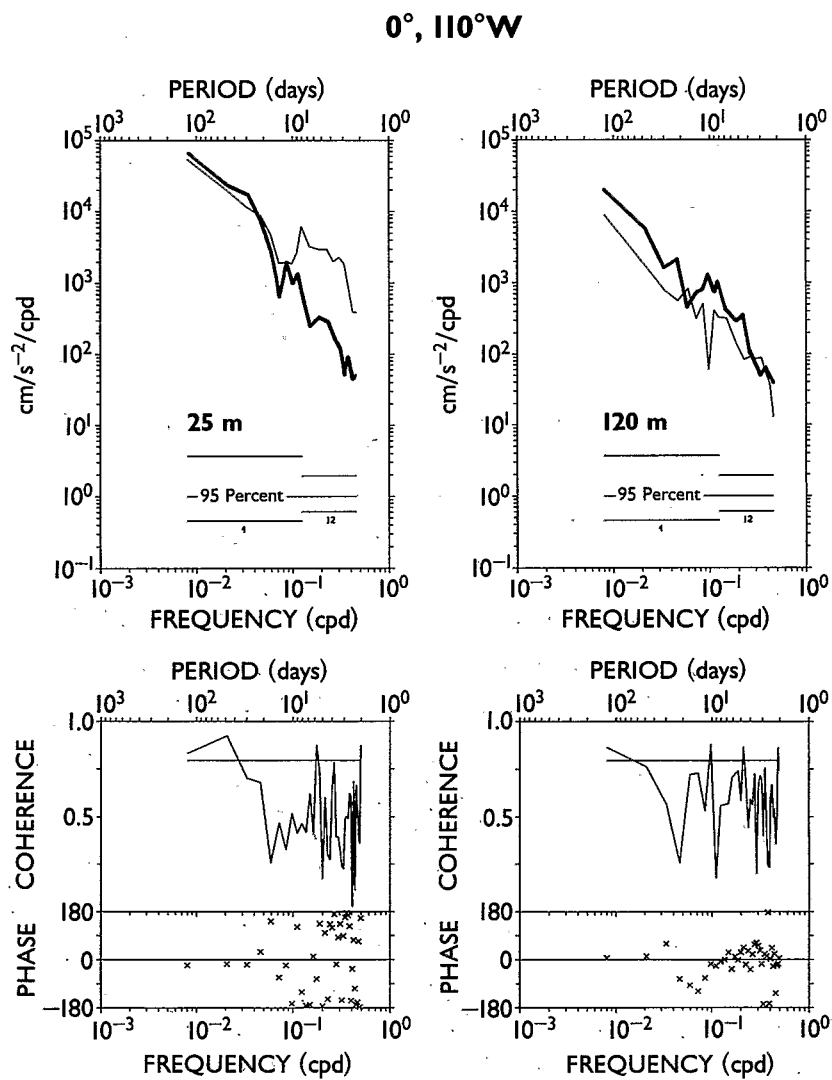


Fig. 4a

Fig. 4b

Fig. 4. Spectra of observed (thick line) and geostrophic (thin line) zonal speed (a) at 110°W (25 m and 120 m) and at (b) 165°E (50 m and 150 m). Coherence between observed and geostrophic currents is shown in each base. Currents are relative to 250 m (110°W) or 300 m (165°E). Error limits on spectra indicate 95% confidence intervals, and the horizontal line on coherence indicates rejection of the null hypothesis (no coherence) with 95% confidence.

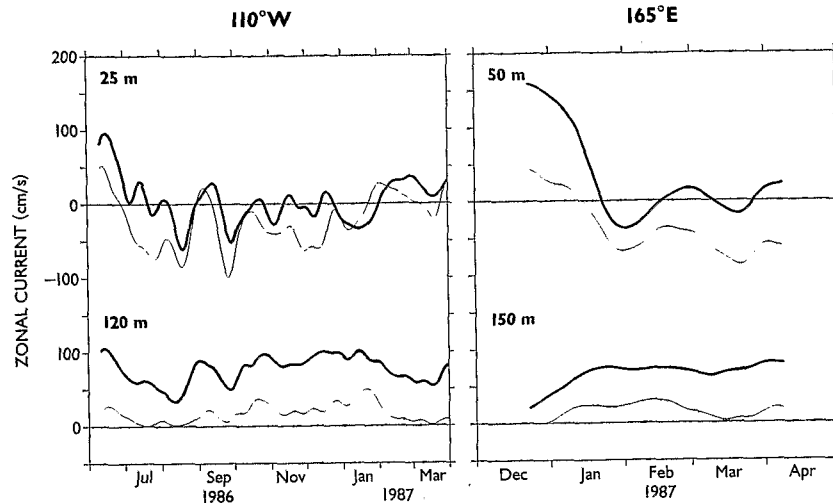


Fig. 5. Time series of observed (thick line) and geostrophic (thin line) zonal speed smoothed by a 21-day Hanning filter. Depths are indicated. Speeds are relative to 250 m (110°W) or 300 m (165°E).

100 m, but the correlation with observed currents is high ( $>0.8$ ). Conversely, below 100 m at 165°E, the differences in standard deviations are smaller, but the correlations are also smaller. The significance of this less consistent performance of the geostrophic approximation at 165°E compared with 110°W is difficult to assess given the relative shortness of the time series.

4. ERROR DISCUSSION

Several sources of uncertainty can contribute to errors in velocities estimated with meridionally differentiated form of the geostrophic equation. Variations of the  $T$ - $S$  relation, particularly in the surface mixed layer, were mentioned earlier. In addition, the meridional and vertical resolution of the measurements can cause errors. The meridional scales of the observations must match the scales of the zonal currents, and the vertical resolution must be sufficient to accurately define the dynamic height at each level. Finally, the geostrophic relation itself is an approximation, and ignored terms in the meridional momentum balance (e.g., friction, nonlinearities, and time dependence) may be important. These error sources are discussed below.

4.1. Horizontal Resolution

If the flow near the equator is in geostrophic balance, then in principle, at the equator  $u$  can be determined from the meridional derivative of (1), i.e., at  $y = 0$ ,

$$\rho\beta u + p_{yy} = -\rho\beta y u_y = 0 \tag{2'}$$

If  $p_{yy}$  is evaluated using finite differences of  $p$  values that are a distance  $O(y)$  from the equator, then we expect an error in (2') of  $O(-\rho\beta y u_y)$ . For an eastward undercurrent centered on or near the equator and finite differences evaluated over  $O(1^\circ)$ ,  $u_y < 0$  for  $y > 0$ , and vice versa. Therefore according to (2'), a finite difference calculation of  $p_{yy}$  underestimates  $u$ . Specifically, at the undercurrent core with  $u_y \approx 50 \text{ cm s}^{-1} \text{ deg}^{-1}$  at 110°W,  $u_y \approx 25 \text{ cm s}^{-1} \text{ deg}^{-1}$  at 165°E, and  $y = 1^\circ$  (i.e., the center of our  $2^\circ$  interval), the underestimate should be about  $50 \text{ cm s}^{-1}$  at 110°W and  $25 \text{ cm s}^{-1}$  at 165°E. These numbers are close to what is actually observed (Figure 6).

Similar arguments can be applied to the surface currents at 110°W and 165°E where the estimated flow is too westward

using (2'). The Doppler current profiler section at 110°W (Figure 1) shows that surface westward flow is weaker at the equator than to the north and not stronger than flow to the south. (Compare with *Lukas and Firing [1984]*, who find that  $u$  at 150–158°W is on a mean less westward on the equator than either to the north or the south.) Thus at 110°W,  $u_y < 0$  for  $y > 0$  and  $u_y \approx 0$  for  $y < 0$ , and a finite difference estimate of  $p_{yy}$  leads to an estimated westward flow at the equator that is too fast. Similar arguments apply at 165°E, where in the mean, westward flow is much stronger to the south and not much different to the north between  $0^\circ$  and  $2^\circ\text{N}$  (Figure 1).

One way to reduce this error is to decrease the meridional grid size in the second-order finite difference scheme. To demonstrate this, we have calculated zonal geostrophic flow at the equator using SURTROPAC and EPOCS CTD sections sub-

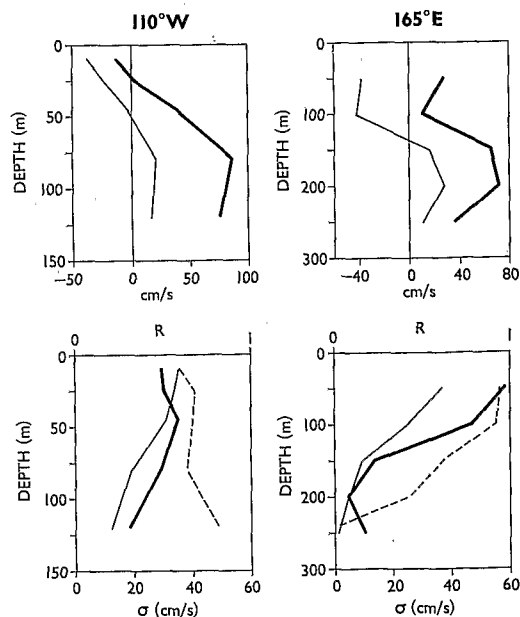


Fig. 6. Profiles of (top) mean and (bottom) standard deviation  $\sigma$  of the observed (thick line) and geostrophically estimated (thin line) low pass filtered zonal velocity (relative to 250 m at 110°W and 300 m at 165°E). Dashed lines in the bottom panels are the correlation coefficient  $R$  between observed and geostrophically estimated current.

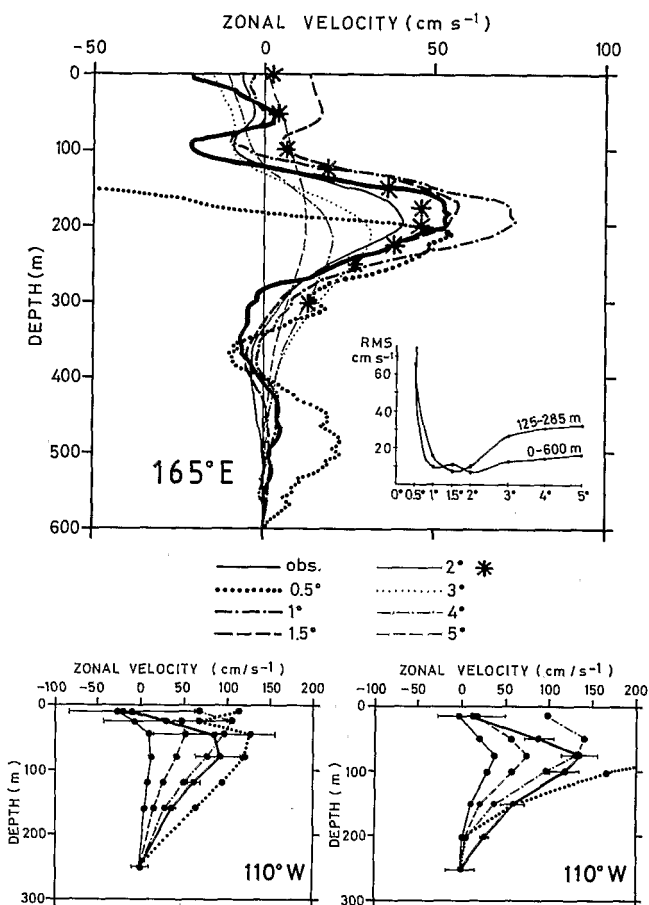


Fig. 7. Profiles of observed and geostrophically estimated zonal current at the equator. At  $165^{\circ}\text{E}$ , geostrophic currents are estimated using CTD station spacings from  $0.5^{\circ}$  to  $5^{\circ}$  latitude. The asterisks indicate the  $2^{\circ}$  spacing calculation repeated using only temperature estimates at the depths of the moored thermistors. At  $110^{\circ}\text{W}$ , geostrophic currents are estimated using station spacings from  $0.5^{\circ}$  to  $2^{\circ}$  latitude. Mean observed currents at the equator are based on profiling current meter measurements at  $165^{\circ}\text{E}$  and on moored current measurements at  $110^{\circ}\text{W}$ .

sampled at various meridional resolutions. Owing to the high-frequency noise on a single transect [Delcroix et al., 1987; Hayes, 1982], our tests have been done over mean transects. Comparison of these observed mean (from profiling current meter data) and the estimated mean from the first SURTROPAC cruises along  $165^{\circ}\text{E}$  is shown in Figure 7. Along  $110^{\circ}\text{W}$ , the acoustic Doppler current profiler has only recently been available. Therefore a similar comparison is done between calculated and observed currents using a mean CTD section and the mean of simultaneous daily averaged moored equatorial current meter measurements. Owing to changes in the depth of moored current measurements over the 11 EPOCS transects, the corresponding CTD and dynamic height data have been averaged over five and six transects, respectively (Figure 7). From these calculations it appears that the optimum horizontal grid size in the second-order finite differences is between  $1^{\circ}$  and  $1.5^{\circ}$  of latitude. This result agrees with Moum et al. [1987], who find that a 100-km scale was optimal for estimating geostrophic zonal flow at the equator on a single intensively sampled transect. As expected, for larger station spacing, the amplitude of the pressure curvature is underestimated, and the inferred equatorial currents are too weak. For smaller station spacing, agreement with observa-

tions also worsens, since the finite difference calculation becomes more affected by high-frequency, small-scale noise.

#### 4.2. Vertical Structure

The vertical resolution of the moored temperature measurements is between 10 and 100 m, similar to a classical hydrocast. Even though sensors are concentrated in the thermocline, the estimated dynamic height from the moorings may miss fine structure that would be seen from continuous temperature profiles. An example of potential error due to coarse vertical resolution is illustrated in Figure 7, which compares equatorial current at  $165^{\circ}\text{E}$  calculated using only CTD measurements at the sensor levels (asterisks) and currents calculated using the full vertical resolution of the CTD (thin line) for stations at  $2^{\circ}$  latitude spacing. Currents tend to be more eastward by about  $10\text{ cm s}^{-1}$  based on data from the depths of the mooring measurements. Although we cannot evaluate the statistical significance of this difference with our relatively sparse data base, vertical temperature resolution of the moorings appears to be less of a limiting factor than meridional resolution in obtaining accurate estimates of geostrophic flow at the equator.

#### 4.3. T-S Variability

In section 2 we noted that use of the mean  $T$ - $S$  relation could introduce errors in the dynamic height and deduced geostrophic current, particularly in the mixed layer. In order to estimate such errors, we have calculated dynamic height time series with  $T$ - $S$  relations which correspond to the 11 EPOCS ( $110^{\circ}\text{W}$ ) and 6 SURTROPAC ( $165^{\circ}\text{E}$ ) sections. At  $110^{\circ}\text{W}$  the standard deviation of dynamic height relative to 250 dbar was 0.5 dyn cm in the surface layer and 0.25 dyn cm below. The currents calculated using (2) have a standard deviation of 11 and  $8\text{ cm s}^{-1}$ , respectively. At  $165^{\circ}\text{E}$  the standard deviation in dynamic height relative to 300 dbar is 1.3 dyn cm in the surface layer and 0.6 dyn cm below, and the standard deviation in the calculated currents,  $25\text{ cm s}^{-1}$  and  $13\text{ cm s}^{-1}$  respectively. Recalling that a 1 dyn cm difference between the equator and  $1^{\circ}$  latitude corresponds to a geostrophic current of  $0.7\text{ m s}^{-1}$ , we expect that the rms errors in dynamic height could induce much larger errors in the geostrophic current if all mooring locations were independent. The relatively small errors in geostrophic current induced by changes in the  $T$ - $S$  relation suggest that these changes are meridionally correlated. The errors in dynamic height at each location have relatively small effect on the curvature and hence on the geostrophic current.

#### 4.4. Neglected Physical Processes

Friction, nonlinearity, and local accelerations are neglected in the geostrophic approximation (equation (1)). Estimated geostrophic currents will therefore be in error to the extent that these processes are important. In this section we examine the probable magnitude of these errors and their impact in our current estimates.

A scaling argument suggests that the magnitude of the error introduced by the neglect of vertical friction is  $O(\tau H/A)$  where  $H$  is the depth scale of flow in the equatorial frictional boundary layer,  $A$  is a vertical eddy viscosity, and  $\tau$  is wind stress. Various models of the layer depth  $H$  exist. For example, Charney [1960] and Stommel [1960] assume that  $H$  coincides with a density-mixed layer. Cane [1979] assumes it is fixed by the nonlinear effects. McPhaden [1981] finds in a continuously

stratified linear model that  $H$  is  $O(A^2/\beta N)^{1/5}$ . Most of these models would suggest  $H$  of  $O(10\text{ m})$  in the eastern Pacific for realistic ranges of parameters. Also, near-surface values of  $A$  in the eastern Pacific are probably  $O(10\text{ cm}^2\text{ s}^{-1})$  [e.g., Gregg et al., 1985]. During periods of strong westerlies,  $A$  may be as large as  $100\text{ cm}^2\text{ s}^{-1}$  in the western Pacific warm pool and  $H$  may be  $O(100\text{ m})$  [McPhaden et al., 1988]. At other times the surface density mixed layer may be shallower [e.g., Lukas and Lindstrom, 1987] and  $A$  may be smaller. If we assume  $\tau$  of  $O(0.1\text{ dyn cm}^{-2})$ ,  $H = O(10\text{ m})$  and  $A = O(10\text{ cm}^2\text{ s}^{-1})$ , then we expect a frictional velocity of  $O(10\text{ cm s}^{-1})$ . Depending on the model and the specific parametric range, this flow will generally be in the direction of the wind at the equator. Thus we would expect to underestimate wind-driven near-surface eastward and westward flows at both locations.

There is another bias due to the neglect of friction that is unique to the equatorial ocean, namely, that baroclinic pressure gradients can balance frictional forces [Stommel, 1960; McPhaden, 1981]. In the meridional momentum balance, this is expressed as

$$p_y = (Av_z)_z \quad (3)$$

In a linear model, (3) is superimposed on the geostrophic balance (1) in the surface boundary layer so that not all the pressure variability can be related to geostrophic currents. For zonal wind forcing, (3) implies a symmetric baroclinic pressure field that is  $O(10\%)$  of the geostrophically balanced pressure field at depths of  $O(10\text{ m})$  below the surface [McPhaden, 1981]. More importantly, meridional winds can set up a cross-equatorial pressure gradient. For  $y = O(100\text{ km})$ ,  $v = O(10\text{ cm s}^{-1})$ ,  $A = O(10\text{ cm}^2\text{ s}^{-1})$  and  $z = O(10\text{ m})$ , the expected sea level height is  $O(1\text{ cm})$  which can lead to an error in the estimate of  $u$  from (1) of  $O(100\text{ cm s}^{-1})$  at  $y = 1^\circ$ . Also, at  $y = 0$ , a nonzero meridional pressure gradient leads to apparent singularities in (1) unless the frictional nature of the pressure signal is taken into account. This type of error is evident in our analyses at  $110^\circ\text{W}$  as seen in Figure 3. Owing to the larger meridional scale of the meridional wind as compared with that of the equatorial currents, this error is largely removed when we use the meridionally differentiated form of the geostrophic balance (2).

A number of authors have used scale analysis to examine the magnitude of nonlinear terms which are not included in (1) and (2) [e.g., Tsuchiya, 1955b; Arthur, 1960; Pedlosky, 1987]. In general, it is found that for reasonable ranges of oceanic parameters, nonlinearity is likely to be only 1–10% of the pressure gradient or curvature. A possible exception to this occurs in the surface layer under the influence of strong meridional wind forcing, where the term  $vv_y$  may be larger [Cane, 1979].

Local accelerations become increasingly important for motion at periods shorter than 1 month near the equator. For example, at periods of about 1 week to 1 month, linear, inviscid mixed Rossby-gravity waves [e.g., Enfield et al., 1987] and instability waves [e.g., Philander et al., 1985] are potentially prominent modes of variability that are not geostrophically balanced. Similarly, at periods of several days to hours, inertia-gravity waves [e.g., Wunsch and Gill, 1976; Eriksen, 1980] and internal tides [Weisberg et al., 1987] are expected to be dominant sources of variability. Thus we would not expect geostrophy to hold on these time scales, consistent with our result (Figure 4) that calculated and observed currents generally become incoherent for periods shorter than 1 month.

## 5. SUMMARY AND CONCLUSIONS

Moored temperature time series on the equator and at  $\pm 2^\circ$  latitude have been used to estimate the geostrophic current on the equator in the eastern ( $110^\circ\text{W}$ ) and western ( $165^\circ\text{E}$ ) Pacific. Currents calculated from the meridionally differentiated form of the geostrophic equation have been compared with observed currents at several depths in the upper 250 m. The results are interpreted as a test of how well the sparse meridional array can be used to infer equatorial zonal currents rather than as a test of the geostrophic balance at the equator. At all locations and depths the mean geostrophically estimated zonal velocity was biased toward the west. At  $110^\circ\text{W}$  this bias increased with depth from about  $25\text{ cm s}^{-1}$  near the surface to about  $60\text{ cm s}^{-1}$  in the undercurrent; at  $165^\circ\text{E}$  the offset was about  $50\text{ cm s}^{-1}$  at all depths. This bias indicates a systematic underestimate of the curvature of the pressure field near the equator. The  $2^\circ$  latitudinal resolution of the moored array is too broad to accurately resolve the near-equatorial mean current structure. Specifically, the finite difference estimate of the second derivative is an average of the zonal current just north and south of the equator which is more westward than the current on the equator. The section data shown in Figure 7 suggest that better estimate of the equatorial curvature requires measurements at about  $1^\circ$  latitude.

Most of the coherent variability between calculated and observed currents was at periods longer than 30 days. Correlation coefficients of time series smoothed with a 21-day Hanning filter varied from about 0.6 to 0.9. These results indicate that much of the month-to-month variability has meridional scales broader than  $2^\circ$ , which is suggestive of the importance of low vertical mode equatorial Kelvin and/or long Rossby waves. At higher frequencies the coherence between observed and computed currents falls off. This intramonthly variability appears to be of smaller meridional scale than  $2^\circ$  and/or ageostrophically balanced.

We found that the meridional pressure gradient at the equator is generally not zero, especially at  $110^\circ\text{W}$ . This gradient is probably balanced by the mean meridional wind stress and leads to unrealistically large cross-equatorial geostrophic shears. An advantage of the second derivative form of the geostrophic relation is that this cross-equatorial pressure gradient is filtered out of the calculation.

In spite of the difficulty in estimating the meridional curvature at the equator, the uncertainties introduced by array spacing,  $T$ - $S$  variability, and physics neglected in the geostrophic approximation, the results presented here indicate that qualitative changes in the magnitude of equatorial zonal currents can be estimated from dynamic height estimates based on moored temperature measurements. Thus it may be possible to derive useful indices of equatorial flow from moored temperature measurements, expendable bathythermograph transects, or satellite altimetric estimates of sea level. Nevertheless, our results indicate that accurate representation of equatorial currents and transports requires direct current measurements.

*Acknowledgments.* The assistance of H. P. Freitag, J. Lynch, M. McCarty, N. N. Soreide, and F. Masia in this analysis is gratefully appreciated. This work was supported, in part, by the Equatorial Pacific Ocean Climate Studies (EPOCS) Project of NOAA ERL, by the U.S. Tropical Ocean-Global Atmosphere (TOGA) Project Office of NOAA OCAR, and by ORSTOM through contracts with Ministère de la Recherche et de l'Enseignement Supérieur (MRES), Programme National d'Etude de la Dynamique du Climat (PNEDC), and ATP Télédétection. NOAA PMEL contribution 1027.

## REFERENCES

- Arthur, R. S., A review of the calculation of ocean current at the equator, *Deep Sea Res.*, 6, 287-297, 1960.
- Cane, M. A., The response of an equatorial ocean to simple wind stress patterns, I, Model formulation and analytical results, *J. Mar. Res.*, 37, 233-252, 1979.
- Charney, J. G., Nonlinear theory of a wind-driven homogeneous layer near the equator, *Deep Sea Res.*, 6, 303-310, 1960.
- Chereskin, T. K., J. N. Moum, P. J. Stabeno, D. R. Caldwell, and C. A. Paulson, Fine-scale variability at 140°W in the equatorial Pacific, *J. Geophys. Res.*, 91(C11), 12,887-12,897, 1986.
- Colin, C., and H. Rotschi, Aspects géostrophiques de la circulation est-ouest dans l'Océan Pacifique équatorial occidental, *C. R. Acad. Sci.*, 271, 929-932, 1970.
- Delcroix, T., G. Eldin, and C. Hénin, Upper ocean water masses and transports in the western tropical Pacific (165°E), *J. Phys. Oceanogr.*, 17(12), 2248-2262, 1987.
- Enfield, D. B., M. P. Cornejo-Rodriguez, R. L. Smith, and P. A. Newberger, The equatorial source of propagating variability along the Peru coast during the 1982-1983 El Niño, *J. Geophys. Res.*, 92(C13), 14,335-14,346, 1987.
- Eriksen, C. C., Evidence for a continuous spectrum of equatorial waves in the Indian Ocean, *J. Geophys. Res.*, 85(C6), 3285-3303, 1980.
- Feely, R. A., R. H. Gammon, B. A. Taft, P. E. Pullen, L. S. Waterman, T. J. Conway, and J. F. Gendron, Distribution of chemical tracers in the eastern equatorial Pacific during and after the 1982-1983 El Niño-Southern Oscillation event, *J. Geophys. Res.*, 92(C6), 6545-6558, 1987.
- Freitag, H. P., M. J. McPhaden, and A. J. Shepherd, Equatorial current and temperature data: 108°W to 110°W; October 1979 to November 1983, *NOAA Data Rep. ERL PMEL-17*, 99 pp., Pac. Mar. Environ. Lab., Seattle, Wash., 1987.
- Gregg, M. C., H. Peters, J. C. Wesson, N. S. Oakey, and T. J. Shay, Intensive measurements of turbulence and shear in the equatorial undercurrent, *Nature*, 318, 140-144, 1985.
- Halpern, D., Observations of annual and El Niño thermal and flow variations at 0°, 110°W and 0°, 95°W during 1980-1985, *J. Geophys. Res.*, 92(C8), 8197-8212, 1987a.
- Halpern, D., Comparison of upper ocean VACM and VMCM observations in the equatorial Pacific, *J. Atmos. Oceanic Technol.*, 4, 84-93, 1987b.
- Hayes, S. P., A comparison of geostrophic and measured velocities in the equatorial undercurrent, *J. Mar. Res.*, 40, suppl., 219-229, 1982.
- Hayes, S. P., J. M. Toole, and L. J. Mangum, Water-mass and transport variability at 110°W in the equatorial Pacific, *J. Phys. Oceanogr.*, 13(2), 153-168, 1983.
- Hidaka, K., Dynamical computation of ocean currents in a vertical section occupied across the equator, *Jpn. J. Geophys.*, 1, 56-60, 1955.
- Jerlov, N. G., Studies of the equatorial currents in the Pacific, *Tellus*, 5, 308-314, 1953.
- Johnson, E. S., L. A. Regier, and R. A. Knox, A study of geostrophy in tropical Pacific Ocean currents during the NORPAX Tahiti Shuttle using a shipboard Doppler acoustic current profiler, *J. Phys. Oceanogr.*, 18, 708-723, 1988.
- Joyce, T., On wind-driven cross equatorial flow in the Pacific Ocean, *J. Phys. Oceanogr.*, 18, 19-24, 1988.
- Kessler, W. S., and B. A. Taft, Dynamic heights and zonal geostrophic transports in the central tropical Pacific during 1979-84, *J. Phys. Oceanogr.*, 17(1), 97-122, 1987.
- Lukas, R., The termination of the equatorial undercurrent in the eastern Pacific, Ph.D. dissertation, 127 pp., Univ. of Hawaii, Honolulu, 1981.
- Lukas, R., and E. Firing, The geostrophic balance of the Pacific equatorial undercurrent, *Deep Sea Res.*, 31, 61-66, 1984.
- Lukas, R., and E. Lindstrom, The mixed layer of the western equatorial Pacific Ocean, in *Proceedings of the 'Aha Huliko'a Workshop*, edited by P. Muller and D. Henderson, pp. 67-94, University of Hawaii, Honolulu, 1987.
- Mangum, L. J., N. N. Soreide, B. D. Davies, B. D. Spell, and S. P. Hayes, CTD/O<sub>2</sub> measurements during the Equatorial Pacific Climate Studies (EPOCS) in 1979, *NOAA Data Rep. ERL PMEL-1*, 643 pp., Pac. Mar. Environ. Lab., Seattle, Wash., 1980.
- McCreary, J. P., A linear stratified model of the Equatorial Undercurrent, *Philos. Trans. R. Soc. London, Ser. A*, 298, 603-635, 1981.
- McPhaden, M. J., Continuous stratified model of the steady state equatorial ocean, *J. Phys. Oceanogr.*, 11, 337-354, 1981.
- McPhaden, M. J., and B. A. Taft, On the dynamics of seasonal and intra-seasonal variability in the eastern equatorial Pacific, *J. Phys. Oceanogr.*, 18, 1713-1732, 1988.
- McPhaden, M. J., H. P. Freitag, S. P. Hayes, B. A. Taft, Z. Chen, and K. Wyrki, The response of the equatorial Pacific to a westerly wind burst in May 1986, *J. Geophys. Res.*, 93(C9), 10,589-10,603, 1988.
- Milburn, H. B., and P. McLain, ATLAS—A low cost satellite data telemetry mooring developed for NOAA's climate research mission, paper presented at the Marine Data Systems International Symposium, Mar. Technol. Soc., New Orleans, La., 1986.
- Moore, D. W., and S. G. H. Philander, Modeling of the tropical oceanic circulation, in *The Sea*, vol. 6, edited by E. D. Goldberg, pp. 319-361, Wiley-Interscience, New York, 1977.
- Moum, J. M., T. K. Chereskin, M. M. Park, and L. A. Regier, Monitoring geostrophic currents at the equator, *Deep Sea Res.*, 34, 1149-1161, 1987.
- Pedlosky, J., An inertial theory of the Equatorial Undercurrent, *J. Phys. Oceanogr.*, 17, 1978-1985, 1987.
- Philander, S. G. H., D. Halpern, D. Hansen, R. Legeckis, L. Miller, C. Paul, R. Watts, R. Weisberg, and M. Wimbush, Long waves in the equatorial Pacific Ocean, *Eos, Trans. AGU*, 66, 154-155, 1985.
- Stommel, H., Wind-drift near the equator, *Deep Sea Res.*, 6, 298-302, 1960.
- Tsuchiya, M., On a simple method of estimating the current velocity at the equator, *J. Oceanogr. Soc. Jpn.*, 11, 1-4, 1955a.
- Tsuchiya, M., On a simple method for estimating the current velocity at the equator, II, *Rec. Oceanogr. Works Jpn.*, 2, 37-42, 1955b.
- Weisberg, R. H., D. Halpern, T. Y. Tang, and S. M. Huang, M<sub>2</sub> tidal currents in the eastern equatorial Pacific Ocean, *J. Geophys. Res.*, 92(C4), 3821-3826, 1987.
- Wunsch, C., and A. E. Gill, Observations of equatorially trapped waves in Pacific sea level variations, *Deep Sea Res.*, 23, 371-390, 1976.
- Wyrki, K., An attempt to monitor the Equatorial Undercurrent, *J. Geophys. Res.*, 88(C1), 775-777, 1983.

S. P. Hayes and M. J. McPhaden, Pacific Marine Environmental Laboratory, NOAA, 7600 Sand Point Way, N.E., Seattle, WA 98115.  
J. Picaut, Groupe SURTROPAC, ORSTOM, B.P. A5, Nouméa, New Caledonia.

(Received June 30, 1988;  
accepted August 8, 1988.)